Supplementary information for Human constraints and scalable design of rotating artificial gravity habitats

Yuzhan Zhang

S1. Scope of the submission supplement

This Supplement contains only material that supports the current self-supporting-annulus formulation, its numerical convergence, uncertainty interpretation, open-human-evidence constraints and computational-credibility case. Superseded full-load magnetic-support calculations are not part of the current design evidence and are therefore not reproduced in full here. The complete historical comparator record remains preserved in the project research archive for auditability.

S2. Legacy topology correction and comparator summary

Early project branches treated the mother-station guideway and magnetic system as if they had to continuously supply the complete radial artificial-weight reaction of each closed annulus. For a continuous closed rotating annulus, that premise is topologically incorrect: nominal centripetal acceleration is closed internally by circumferential tension. The mother-side electromagnetic system is therefore retained only for centering, gap regulation, noncontact tangential drive, disturbance rejection and fault management.

Table 1: Status of superseded comparator branches. These branches are preserved in the research archive but are not current design evidence.

Legacy branch	Why it was useful	Current status
Full-load guideway / magnetic support	Exposed force-density, stiffness, alignment and segmentation burdens under the earlier load path	Superseded for continuous self-supporting A/B annuli; retained only as a comparator for discrete or non-self-supporting vehicle branches
PM-biased attractive support	Quantified copper-power and negative-stiffness control gates	No longer the preferred nominal support interpretation; zero/near-zero-bias active centering is the current functional role
Moving ferromagnetic reaction rail	Revealed self-mass feedback, segmentation and eddy-loss penalties	Demoted; high-conductivity continuous moving back-iron is rejected by the current magnetoquasistatic gate
Rigid/sliding touchdown	Established a conservative upper-bound braking and rub-energy scale	Replaced as the primary fault model by flexible-annulus rolling-containment dynamics
Full-ring C-buffer sink	Tested whether a third annulus could absorb complete habitat momentum	Rejected as a preferred role; C is a short-time local transient buffer while paired A/B braking handles large momentum redistribution

The correction changes the engineering question rather than eliminating it. Current submission evidence therefore focuses on pressure-shell mass, low-force electromagnetic centering, flexible rolling contact, paired momentum management, general scaling laws and the uncertainty/credibility of those models. Historical equations, figures and sensitivity scans for the superseded branches are available in the archived full legacy supplement distributed with the reproducibility record.

S3. High-fidelity convergence and sensitivity

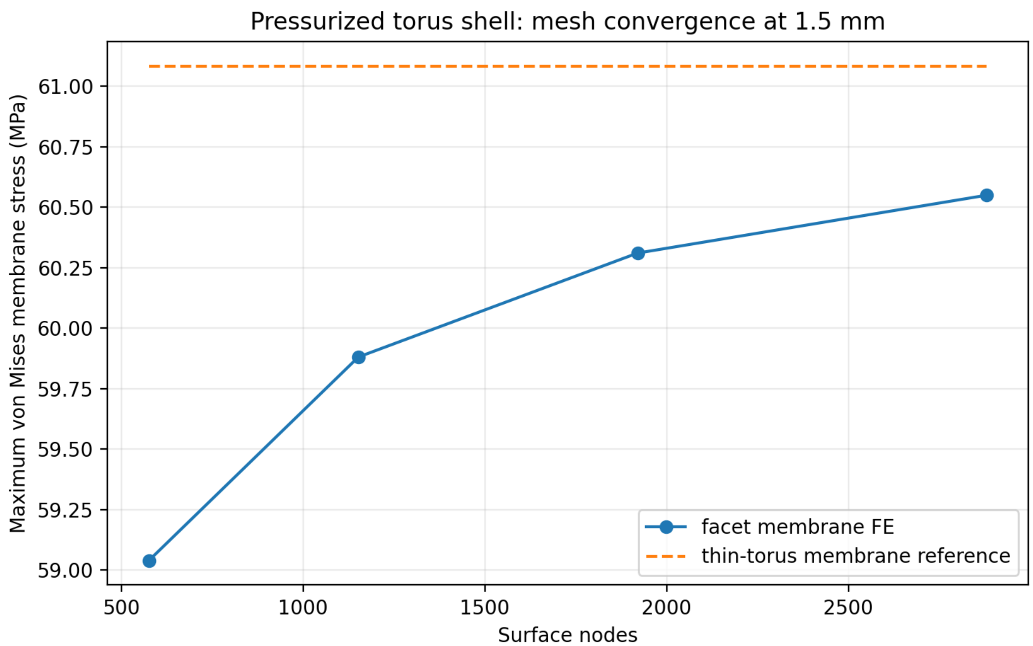

Figure 1: Pressure-torus membrane mesh convergence.

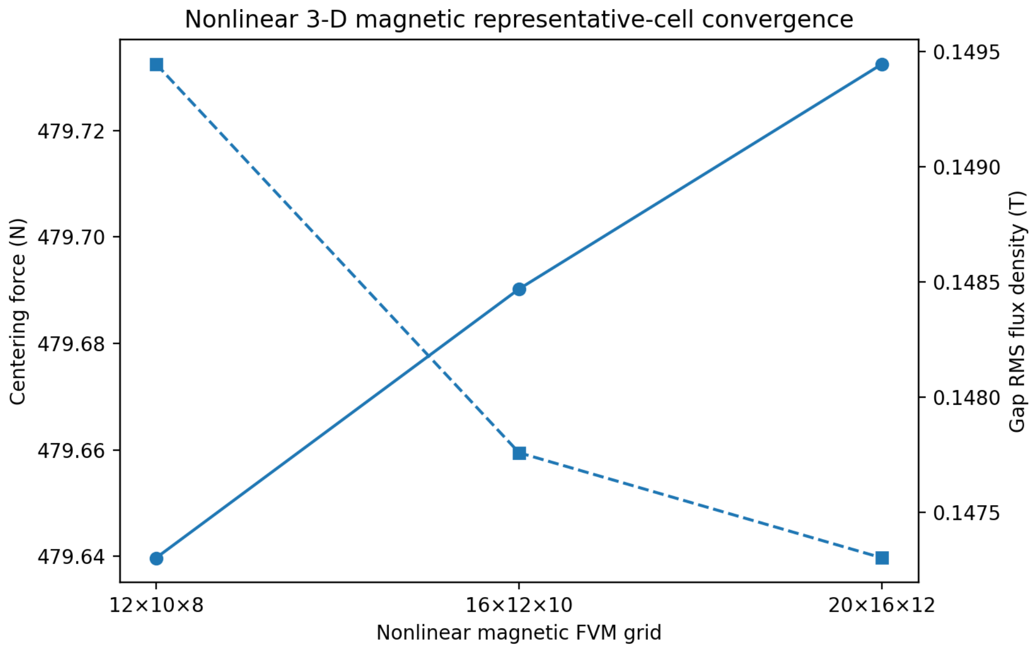

Figure 2: Nonlinear magnetic representative-cell grid convergence.

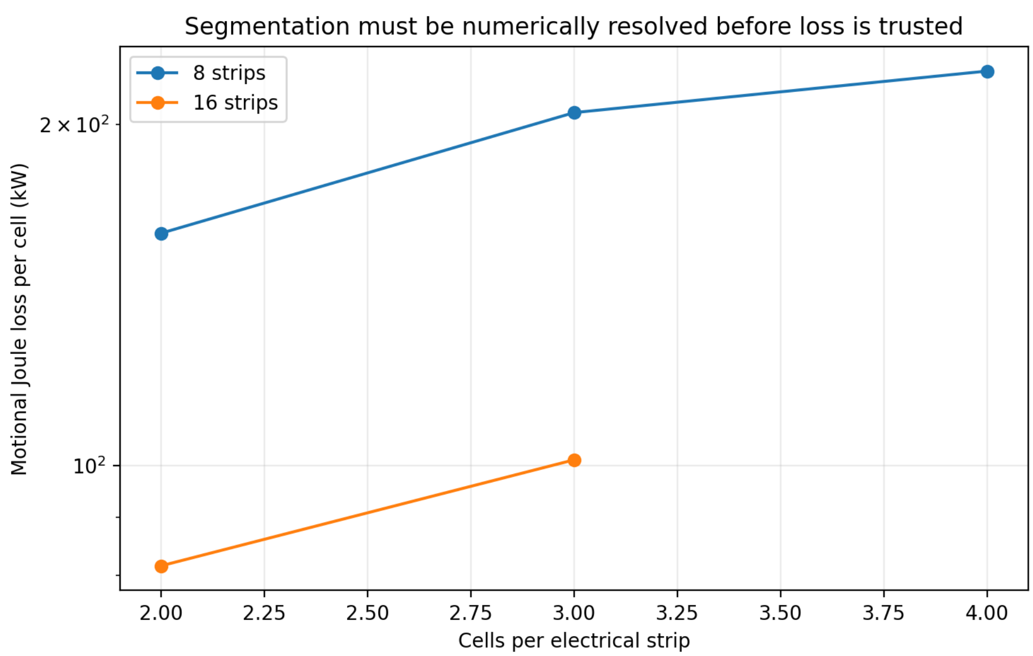

Figure 3: Electrical-strip numerical resolution sensitivity.

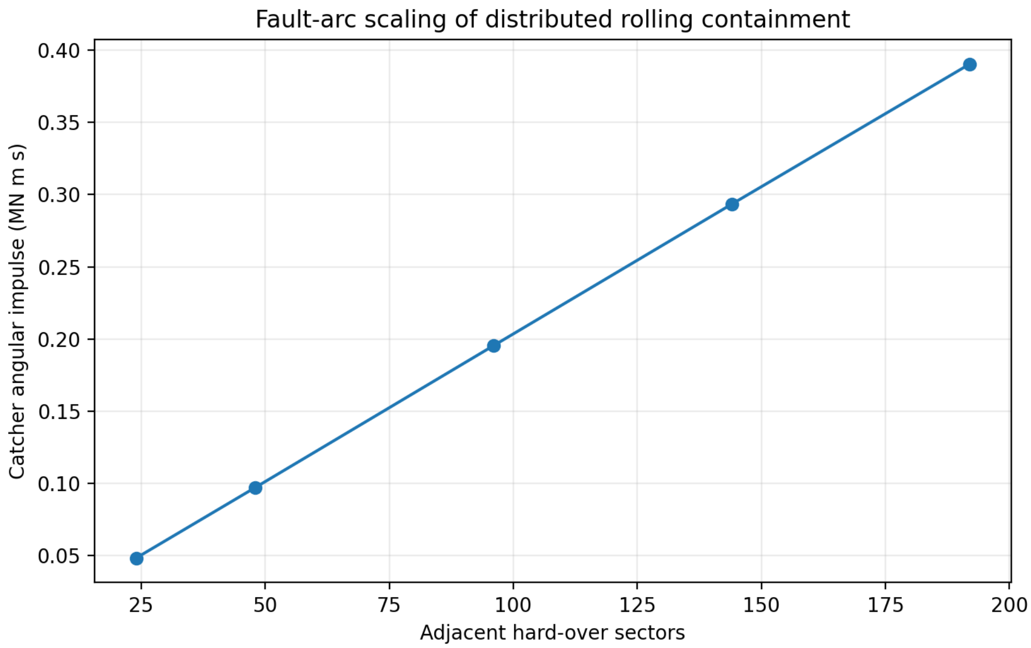

Figure 4: Fault-arc scaling of catcher angular impulse.

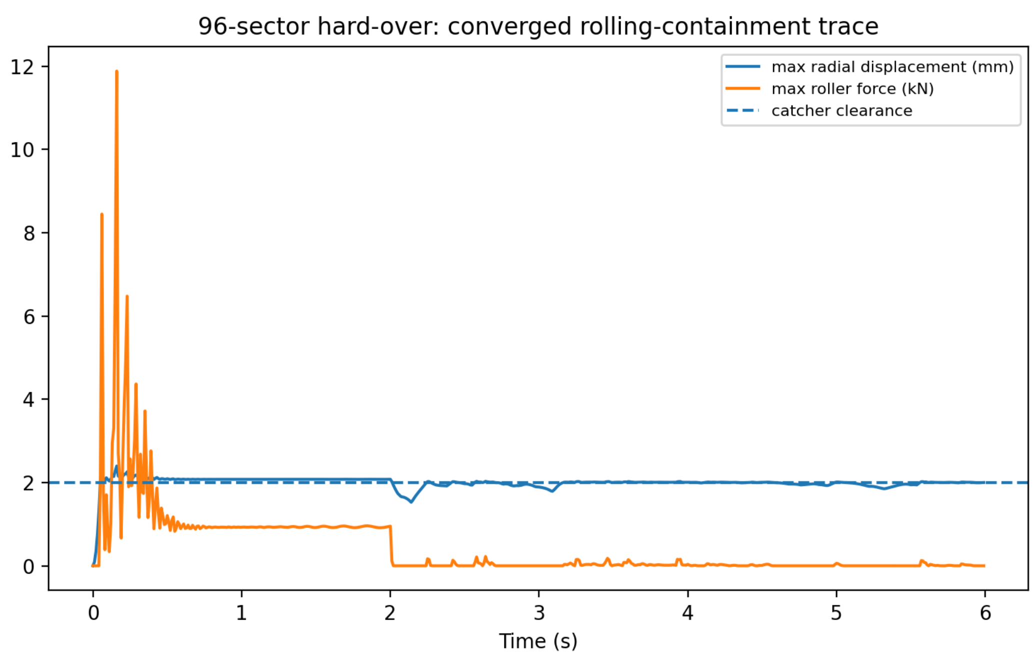

Figure 5: Representative converged rolling-containment trace.

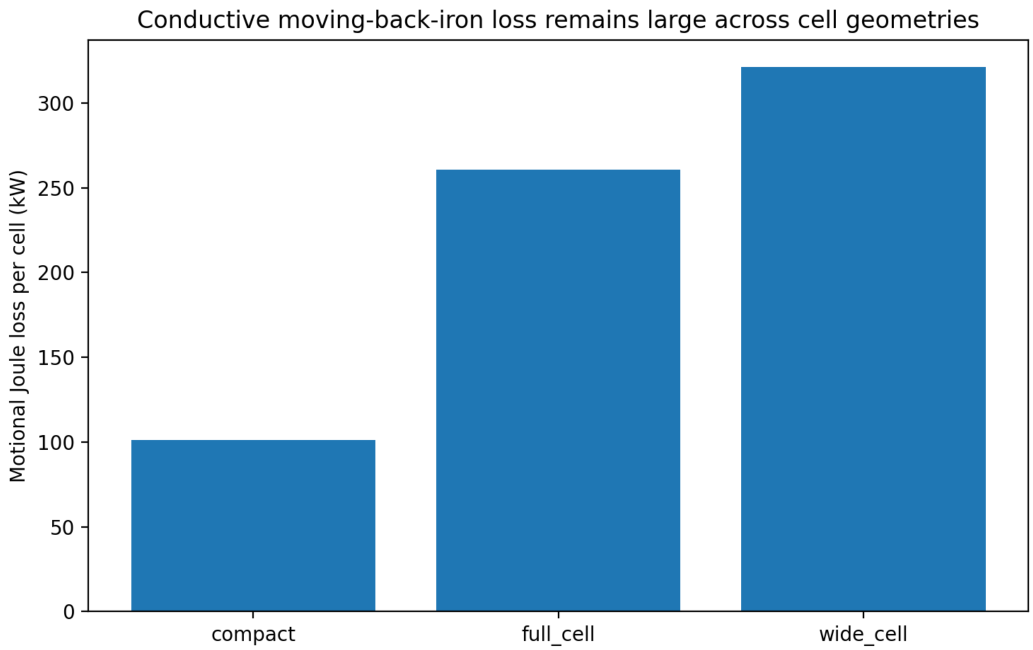

Figure 6: Moving-conductor geometry sensitivity at steel-like conductivity.

S4. Layered fault-management visualization

The current fault-management sequence is summarized below as a communication aid. The diagram does not add a new controller model: the catcher impulse, C-buffer range, detection-latency example and mother-station residual are the same screening quantities reported in the main manuscript and numerical results. In particular, the C ring is a short-time internal buffer and is not sized to absorb the complete steady angular momentum of a crewed annulus.

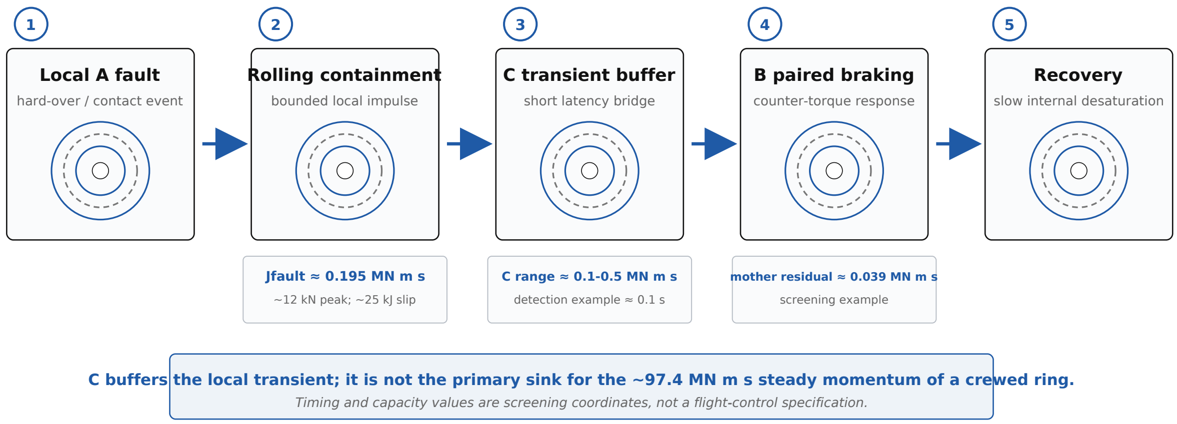

Figure 7: Layered transient-management sequence used to interpret the A/B/C fault screen: local A-annulus fault, rolling containment, short-time C buffering, paired B braking and slow recovery. Timing and capacity values shown are screening coordinates, not a flight-control specification.

S5. Open-evidence constraints, uncertainty and credibility

This section documents the evidence and credibility material added after the engineering-figure integration. It uses only immediately accessible group-level human evidence and public archive metadata. No individual-participant biomedical dataset that requires credentialing, privacy approval or application is used.

S5.1 Open human evidence envelope

The physiological model is constrained by several endpoints that do not all respond in the same direction. AGBRESA provides an acute vascular calibration and selected bone/BMAT protection signals, whereas BRACE provides muscle, cardiorespiratory and orthostatic constraints. The intended use is cross-study calibration and falsification of overly simple gravity-dose assumptions, not pooled treatment efficacy or individual prediction [1, 2, 3, 4, 5].

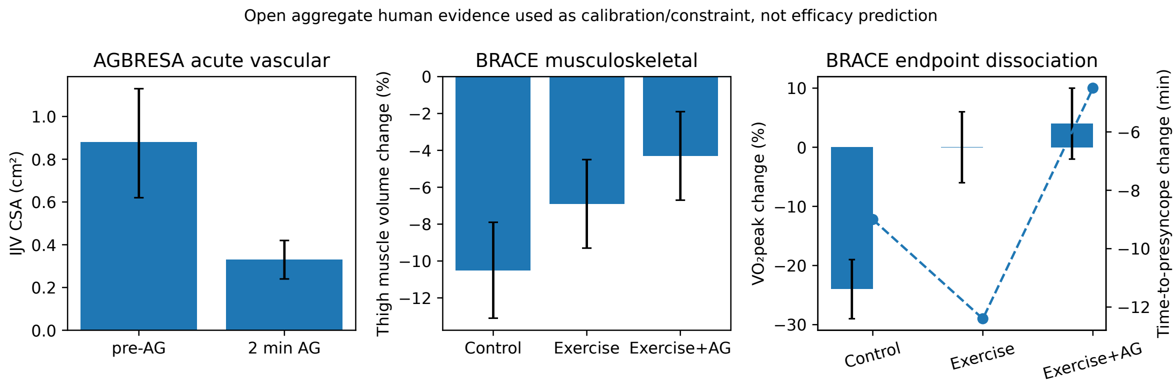

Figure 8: Selected openly accessible aggregate human evidence used as calibration or constraint. Endpoints are intentionally shown in their native units and are not combined into a single efficacy score.

S5.2 Scenario uncertainty and general design use

The pressure-ring uncertainty screen varies shell thickness, internal pressure, aluminum-like density and internal payload over explicit research ranges. The resulting 5–50–95% intervals are scenario envelopes rather than statistical confidence intervals or reliability distributions.

For the C-buffer screen, a similarly broad fault-extent/severity ensemble produces a median local impulse of about 0.216 MN m s and a scenario capacity-exceedance fraction of about 0.31 when C capacity is sampled over 0.1–0.5 MN m s. This fraction is not an estimated failure probability. It only demonstrates that C capacity should remain fault-tree-derived until actuator fault severity and frequency are established.

S5.3 Computational credibility case

The credibility organization follows the public NASA-STD-7009B categories of verification, validation, input pedigree, uncertainty and robustness, with NASA-HDBK-7009B used as implementation guidance [6, 7]. Ratings are internal project assessments and do not indicate NASA certification.

Three independent checks constrain the current solvers without relying on the same numerical pathway: the finest pressure FE result is within about 0.9% of the thin-torus membrane limit; the

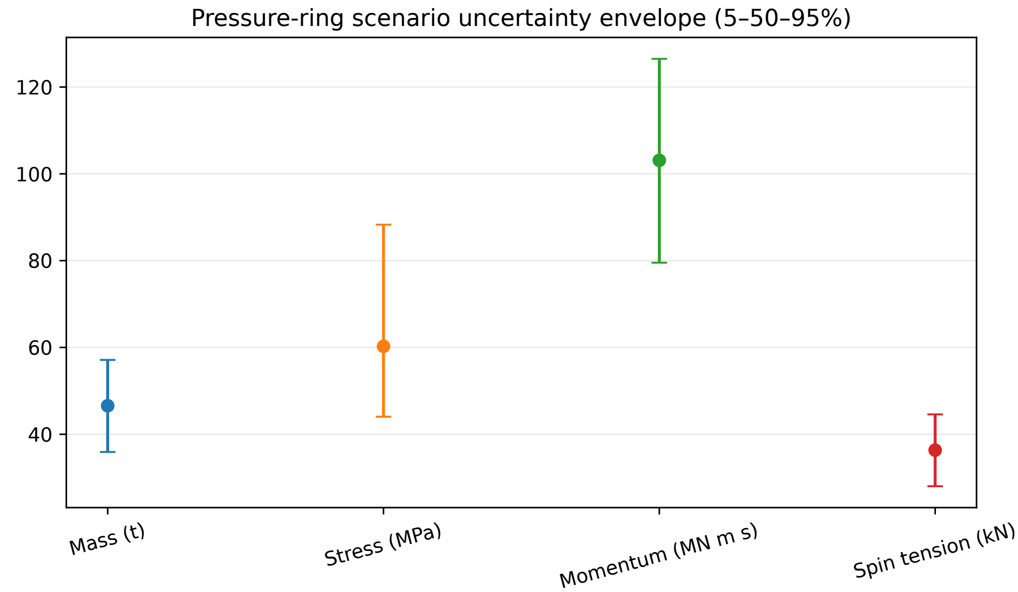

Figure 9: Pressure-ring scenario uncertainty envelope. The sampled inputs are design-space priors, so the plotted percentiles must not be interpreted as manufacturing or failure probabilities.

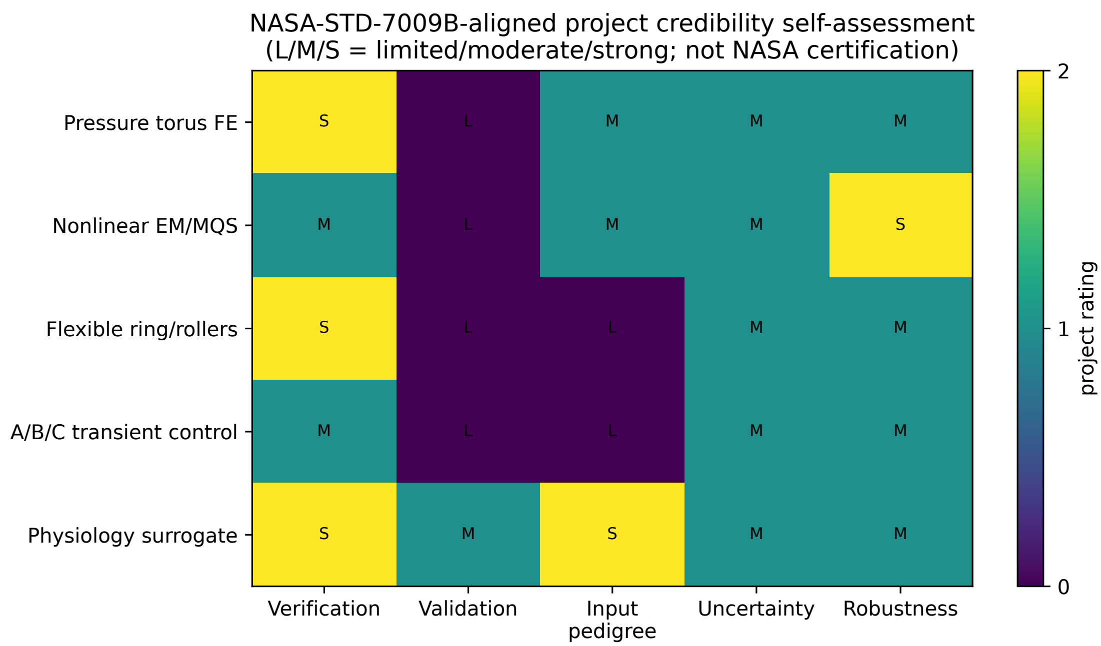

Figure 10: Project credibility self-assessment by model family. Verification is generally stronger than physical validation, which remains the dominant unresolved engineering evidence gap.

flexible-contact angular impulse matches $MR\Delta v$ to numerical precision; and the low-reaction-field MQS conductivity sweep recovers the expected unit log–log loss/conductivity slope. These are verification evidence, not substitutes for experiment.

S5.4 Architecture mechanism comparator

Table 2 is intentionally descriptive rather than a scalar ranking. It states the dominant system-level exchange for four common AG architecture families.

Table 2: Mechanism-level architecture comparison; no cost or TRL ranking is implied.

Architecture	Non-rotating work volume	Momentum-management mode	Principal system exchange
Whole-station rotation	Limited unless separate hub	Vehicle spin or counter-rotor	Continuous large-volume AG at the cost of high rotating mass/inertia and rotating interfaces
Short-arm centrifuge	Yes	Local rotor reaction torque	Low moving mass and individualized exposure, but high rpm and body-length gravity gradient
Rotating habitat + counterweight	Yes	Counterweight / tether or paired rotating mass	Separates some stationary functions from AG, but requires dynamic balance and transfer interfaces
Stationary-frame counter-rotating annuli	Yes	Paired A/B cancellation plus local C transient buffer	Schedulable AG and persistent 0-g work volume, exchanged for moving pressure-ring momentum, centering and fault containment

References

[1] K. Marshall-Goebel et al., Effects of artificial gravity on the vascular system during 60 days of strict head-down tilt bedrest, Journal of Applied Physiology 141 (2026) 120–129. https://doi.org/10.1152/japplphysiol.00667.2025.

[2] K. Culliton et al., Artificial gravity protects bone and prevents bone marrow adipose tissue accumulation in humans during 60 d of bed rest, Journal of Bone and Mineral Research 40 (2025) 1218–1227. https://doi.org/10.1093/jbmr/zjaf119.

[3] M. Mandić et al., Limited musculoskeletal benefits of artificial gravity combined with cycling during bed rest: results from the BRACE study, Experimental Physiology (2026). https://doi.org/10.1113/EP093145.

[4] E.T. Hedge, C.G. Bryans, C.J. Mastrandrea, C. Siebenmann, A.R. Hargens, L.L. Karlsson, R.L. Hughson, D. Linnarsson, Exercise during artificial gravity preserves cardiorespiratory fitness but not orthostatic tolerance following 60 days of head-down bed rest (BRACE), Journal of Applied Physiology (2025). https://doi.org/10.1152/japplphysiol.00224.2025.

[5] European Space Agency, BRACE 2023 - Bed Rest with Artificial gravity and Cycling Exercise - Baseline Data, HRE Data Archive, version 1.0, 2025, DOI 10.57780/esa-3nbdkc9.

[6] National Aeronautics and Space Administration, NASA-STD-7009B, Standard for Models and Simulations, 5 March 2024. https://standards.nasa.gov/standard/nasa/nasa-std-7009 (accessed 4 September 2026).

[7] National Aeronautics and Space Administration, NASA-HDBK-7009B, NASA Handbook for Models and Simulations: An Implementation Guide for NASA-STD-7009B, 3 February 2026. https://standards.nasa.gov/standard/nasa/nasa-hdbk-7009 (accessed 4 September 2026).